Acta Pharmaceutica Sinica B 2025;15(1):611−626

Chinese Pharmaceutical Association
Institute of Materia Medica, Chinese Academy of Medical Sciences

Acta Pharmaceutica Sinica B

www.elsevier.com/locate/apsb
www.sciencedirect.com

ORIGINAL ARTICLE

Unlocking the role of wound microbiome in diabetic, burn, and germ-free wound repair treated by natural and synthetic scaffolds

Zeyu Xu[a], Lixiang Zhang[a], Qinghan Tang[a], Chenxi Yang[a], Xiaotong Ding[a], Ziyu Wang[b,c], Rizhong Huang[a], Ruihan Jiang[a], Joannake Maitz[d,e], Huaikai Shi[f], Xin Yan[g], Mei Dong[a,*], Jun Chen[a,h,*], Yiwei Wang[a,g,h,*]

[a]*Jiangsu Provincial Engineering Research Center of TCM External Medication Development and Application, School of Pharmacy, Nanjing University of Chinese Medicine, Nanjing 210023, China*
[b]*School of Life and Environmental Sciences, the University of Sydney, NSW 2006, Australia*
[c]*Charles Perkins Centre, the University of Sydney, NSW 2006, Australia*
[d]*ANZAC Research Institute, Concord Hospital, University of Sydney, NSW 2138, Australia*
[e]*Burns and Reconstructive Surgery, Concord Hospital, NSW 2138, Australia*
[f]*Asbestos and Dust Diseases Research Institute, Concord, NSW 2138, Australia*
[g]*Department of Burns and Plastic Surgery, Nanjing Drum Tower Hospital, Affiliated Hospital of Medical School, Nanjing University, Nanjing 210003, China*
[h]*Jiangsu Collaborative Innovation Center of Chinese Medicinal Resources Industrialization, School of Pharmacy, Nanjing University of Chinese Medicine, Nanjing 210023, China*

Received 10 May 2024; received in revised form 17 August 2024; accepted 20 August 2024

KEY WORDS

Natural scaffolds;
Synthetic scaffolds;
MatriDerm®;
Polycaprolactone;
Wound commensal microbiome;
Wound healing;

Abstract In current clinical practice, various dermal templates and skin substitutes are used to enhance wound healing. However, the role of wound commensal microbiome in regulating scaffold performance and the healing process remains unclear. In this study, we investigated the influence of both natural and synthetic scaffolds on the wound commensal microbiome and wound repair in three distinct models including diabetic wounds, burn injuries, and germ-free (GF) wounds. Remarkably, synthetic electrospun polycaprolactone (PCL) scaffolds were observed to positively promote microbiome diversity, leading to enhanced diabetic wound healing compared to the natural scaffolds Integra® (INT) and MatriDerm® (MAD). In contrast, both natural and synthetic scaffolds exhibited comparable effects on the diversity

*Corresponding authors.
E-mail addresses: meidong707@njucm.edu.cn (Mei Dong), chenjun75@njucm.edu.cn (Jun Chen), yiweiwang@njucm.edu.cn (Yiwei Wang).
Peer review under the responsibility of Chinese Pharmaceutical Association and Institute of Materia Medica, Chinese Academy of Medical Sciences.

https://doi.org/10.1016/j.apsb.2024.08.024

Immune response;
Inflammation

of the microbiome and the healing of burn injuries. In GF wounds with no detectable microorganisms, a reversed healing rate was noted showing natural scaffold (MAD) accelerated wound repair compared to the open or the synthetic scaffold (PCL) treatment. Furthermore, the response of the wound commensal microbiome to PCL scaffolds appears pivotal in promoting anti-inflammatory factors during diabetic wound healing. Our results emphasize that the wound commensal microbiome, mediated by different scaffolds plays an important role in the wound healing process.

1. Introduction

Skin wounds such as chronic wounds (*e.g.*, diabetic ulcers) and acute wounds (*e.g.*, burn injuries) exhibit a complex healing process, which is characterized by delayed wound closure. These are especially prevalent in elderly individuals and patients who suffer from diabetes, vascular disease, obesity, malnutrition, or a combination of these factors[1]. Diabetic ulcers (DUs) are severe and common complications of diabetes with a 25% incidence rate, which significantly affects patients' quality of life due to prolonged healing times, high infection, high amputation rate, and increased medical costs[2]. Burn injuries are normally caused by heat, radiation, and chemical sources[3]. A recent report indicated that approximately a million patients are affected by burn injuries in the United States each year, costing 4 billion U.S. dollars[4].

A variety of dermal templates and skin substitutes containing biomaterials have been developed to treat different wounds[5-7]. The primary goal of these scaffolds is to control infection, enhance wound repair, and stimulate skin regeneration while minimizing the long-term consequences of scarring[8]. Both natural and synthetic polymers are used as matrices in dermal templates and skin substitutes. Natural polymers such as collagen, elastin, alginate, and cellulose are soluble in aqueous solutions and biodegradable *in vivo*[9]. Collagen and elastin, as the major components in the skin, have been fabricated into sponges, films, and hydrogels to facilitate wound healing due to their favorable biocompatibility[10-14]. Commercially available collagen-based dermal templates, such as crosslinked Integra® (INT, Integra® LifeSciences Corporation, Plainsboro, NJ, USA) and non-crosslinked MatriDerm® (MAD, Dr. Otto Suwelack Skin & Health Care AG, Billerbeck, Germany), are widely utilized in clinical settings to treat acute and chronic wounds[15]. However, the poor physical properties of natural polymers pose limitations for medical applications. In contrast, synthetic polymers, including an FDA-approved polyester, polycaprolactone (PCL), and poly(lactic-*co*-glycolic acid) (PLGA)-based scaffolds, have been developed as durable and effective skin substitutes that enhance the mechanical strength[16].

The skin serves as the habitat for the microbiome, with the commensal microbiome on the skin interacting with the host to maintain the integrity of the skin barrier. Disruptions to the homeostasis of the skin microbiome can lead to the occurrence of psoriasis and atopic dermatitis[17-19]. The colonization of wound microorganisms can stimulate wound infection as well as biofilm formation. Moreover, infection impairs diabetic and chronic wound healing and contributes to severe complications such as osteomyelitis and amputation[20]. In diabetic wounds, *Staphylococcus* is the most common microorganism, and the main clinical treatment for diabetic wounds is to reduce or inhibit the quantity of *Staphylococcus*[21]. However, a recent report revealed that the complete removal of wound microorganisms from diabetic ulcers using combined antibiotics resulted in the reduction of the wound commensal microbiome and significantly delayed wound closure[22]. This finding explains the poor outcomes associated with antibiotic use in diabetic ulcer treatment[23], suggesting that regulating the wound commensal microbiome is crucial for promoting diabetic wound healing[22]. In burn injuries, which are considered acute wounds, the microbiome can be re-instated from wound edges[24]. Acute wounds typically lack a diverse microbiome, but the reinstatement of microbiota into these wounds can significantly impact both the local healing process and systemic gut dysbiosis[25]. Several factors are known to influence the commensal microbiome of wounds, including the use of antibiotics, aging, diabetes, autoimmunity, and immunosuppression[26,27]. However, the effects of various dermal templates and skin substitutes on the wound commensal microbiome in relation to wound healing processes have not yet been reported. A recent study investigated how the host microbiome influences the foreign body response following biomaterial implantation[28], revealing that germ-free mice exhibited less fibrous tissue deposition, reduced host cell recruitment, and differential expression of inflammatory markers. These findings suggest that the microbiome can reversely alter the performance of biomaterial scaffolds.

In this study, we investigated the wound commensal microbiome in response to commercial natural scaffolds including INT and MAD, and synthetic electrospun scaffolds fabricated from PCL and PLGA, and their effects on various wound healing processes. To our knowledge, this is the first exploration of wound commensal microbiome responses to varying scaffolds. The findings of this study will aid in the future design of innovative dermal templates and skin substitutes for diverse wound types.

2. Materials and methods

2.1. Materials

Integra® (INT), a porous dermal template composed of crosslinked native bovine collagen type I was obtained from Integra® LifeSciences Corporation (Plainsboro, NJ, USA). MatriDerm® (MAD), a porous dermal regenerative template made of native bovine collagen types I, II, and V, and 3% α-elastin without crosslinking was provided by Dr. Otto Suwelack Skin & Health Care AG (Billerbeck, Germany). PCL (Mw = 80,000 g/mol) was purchased from Sigma−Aldrich (St. Louis, MO, USA). PLGA

(Mw = 100,000 g/mol, LA: GA = 50:50) was kindly provided by Jinan Daigang (Jinan, China).

2.2. Fabrication of electrospun PCL and PLGA scaffolds

Electrospun PCL and PLGA scaffolds were produced as previously described[29]. Polymers were dissolved in 1,1,1,3,3,3-hexafluoro-2-propanol (HFP) (Sigma Aldrich, St. Louis, MO, USA) at 10% *w/v* for PCL and 13% *w/v* for PLGA. Subsequently, 0.5 mL of the PCL or PLGA solution was used for electrospinning. After 30 min of air drying, the scaffolds were removed from the collector and stored at room temperature.

2.3. Analysis of surface morphology

The surface morphologies of INT, MAD, electrospun PCL, and electrospun PLGA scaffolds were examined by scanning electron microscopy (SEM) (Tescan Maia3 Gmu, Tescan Orsay Holding, CZ). The samples were coated with platinum at 40 nm prior to scanning by SEM at a voltage of 20 kV. The surfaces of all four scaffolds were further analyzed using Fiji ImageJ version 2.0 (National Institutes of Health, Bethesda, MD, USA)[30].

2.4. In vivo diabetic wound healing model

Male *db/db* mice, 12 weeks old, weighing 40−50 g each (n = 100, 5/group/time point including Days 3, 7, 14, and 21), were obtained from GemPharmatech (Nanjing, China). All animals were housed in standard approved cages with free access to water in a specific-pathogen-free (SPF) facility at Nanjing University of Chinese Medicine. The environment was closely controlled at 24−26 °C and 44%−46% humidity under a 12:12 h light/dark cycle with lights on at 6 a.m. All experimental procedures were executed according to the protocols approved by the Animal Ethics Committee, Nanjing University of Chinese Medicine (ethic No. 202203A072).

Db/db mice were under general anesthesia (3% isoflurane) during the surgery, where a small wound of 1 cm^2 was created. Subsequently, all animals were randomly assigned to one of the following groups: NC (open wounds), INT, MAD, PCL, or PLGA scaffolds, respectively. Post-injury, animals were given 1 mL of warm resuscitative intraperitoneal saline and analgesia (intraperitoneal carprofen 5 mg/kg). All animals were then housed individually and monitored daily for any signs of distress or changes in physical appearance. Wound sizes on Days 0, 3, 7, 14, and 21 were measured. Mice were euthanized by cervical dislocation at each time point, and the wound tissues were harvested for histology and molecular analysis. Blood was collected *via* cardiac puncture prior to euthanizing, and serum was isolated and stored at −80 °C until further analysis.

2.5. In vivo burn wound healing model

Male BALB/c mice, 12 weeks old, weighing 25−30 g each (n = 30, 5/group/time point including Days 3 and 7), were purchased from GemPharmatech (Nanjing, China). All experimental procedures were executed according to the protocols approved by the Animal Ethics Committee, Nanjing University of Chinese Medicine (ethic No. 202305A013).

A mouse model of a small burn was previously established[31]. Briefly, a 1 cm^2 brass was heated to 230 °C before being applied to the shaved skin and allowed to rest on the dorsum area for 9 s to produce a full-thickness burn. Immediately after the burn injury, 1 mL of warm resuscitative intraperitoneal saline and analgesia (intraperitoneal carprofen 5 mg/kg) were administered. Two days post-burn injury, the damaged skin was removed surgically to create a 1 cm^2 burn wound. Thereafter, all animals were randomly assigned to one of the following groups: NC, MAD, and PCL scaffolds. Analgesia was provided daily for 4 days after the burn injury. Wound sizes on Days 0, 3, and 7 were measured. Wound tissues were harvested for histology and molecular analysis, respectively.

2.6. In vivo germ-free (GF) wound healing model

Male GF BALB/c mice, 12 weeks old, weighing 25−30 g each (n = 30, 5/group/time point including Days 3 and 7), were bred and maintained in special plastic isolators (GemParmatech, Nanjing, China), housed under a strict 12 h:12-h light−dark cycle (lights on at 08:00). The animals were supplied with a 50-kGy irradiated sterile pelleted normal chow diet, and autoclaved tap water *ad libitum*. All GF mice were tested for fecal bacteria, viruses, and fungus contamination by facility staff to ensure that the GF unit was indeed sterile, and all experimental procedures were executed according to the protocols approved by the Animal Ethics Committee, GemPharmatech (ethic No. GPTAP20230621-4).

GF mice were generally anesthetized by intraperitoneal injection of an anesthetic (ketamine/xylazine cocktail at a dose of 2 mL of ketamine and 50 μL of xylazine diluting with 7.95 mL of saline, 0.1 mL/10 g). A 1 cm^2 wound was created surgically. Thereafter, all animals were randomly assigned to one of the experimental groups: NC, MAD, or PCL scaffolds, respectively. Post-injury, animals were given 1 mL of warm resuscitative intraperitoneal saline and subcutaneous injection analgesia was given immediately after the injury. Wound sizes were measured on Days 0, 3, and 7. Wound tissues were harvested and collected for histology and molecular analysis.

2.7. 16S rRNA gene sequences

The wound area was wiped with a sterile cotton swab 20 times, followed by storage in a sterile and enzyme-free centrifuge tube at −80 °C. Wound microbiome samples collected from *db/db* mice and burn injury mice were sent to Majorbio Bio-Pharm Technology (Shanghai, China) for Illumina 16S rRNA gene sequencing. Briefly, genomic DNA was extracted from wound samples, and microbial community 16S rRNA libraries were generated as previously described[22]. After the PCR reaction, purified amplicons were pooled equimolarly and paired-end sequenced on an Illumina MiSeq PE300 platform (Illumina, San Diego, CA, USA) according to the protocols. Raw FASTQ files were then demultiplexed using an in-house perl script and quality-filtered by fastp version 0.19.6[32] and merged by FLASH version 1.2.11[33]. The optimized sequences were clustered into operational taxonomic units (OTUs) using UPARSE 11[34] with a 97% sequence similarity level. Based on the OTU abundance profile, α-diversity and β-diversity analyses were performed and analyzed using the online platform of Majorbio Cloud Platform (www.majorbio.com). Within-sample α-diversity was assessed using Chao 1 and Shannon indices. The Chao 1 index is a metric of richness that estimates the total number of species in samples. The higher its value, the more abundant the α-diversity[35]. The Shannon index combines richness and evenness; the higher its value is, the more abundant the α-diversity[35]. Between-sample β-diversity was visualized by a principal coordinate analysis (PCoA) plot based on the binary_jaccard distance. Statistical significance α-diversity was determined using the

Kruskal–Wallis H test, and β-diversity using ANOSIM analysis (*unclassified* indicates microbiome on the genus level, but its name is not included in the database and can only be determined on the phylum level or family level). The relative abundance of key microbiomes on the phylum and genus level was analyzed using the Kruskal–Wallis H test. Sequencing data including all field and incubated samples have been submitted to the NCBI Sequence Read Archive (accession No. SRP492073).

2.8. Metagenomic sequencing

Wound microbiome samples were used to extract total genomic DNA with the FastDNA™ Spin Kit for Soil (MP Biomedicals, Santa Ana, CA, USA). The concentration of the extracted DNA was determined with TBS-380 and NanoDrop2000, respectively. DNA quality was checked on a 1% agarose gel. The DNA extract was fragmented to an average size of about 400 bp using Covaris M220 (Gene Company Ltd., Hong Kong, China) for paired-end library construction. The paired-end library was constructed using NEXTFLEX Rapid DNA-Seq (Bioo Scientific, Austin, TX, USA). Paired-end sequencing was performed on Illumina Novaseq 6000 (Illumina Inc., San Diego, CA, USA) using the NovaSeq 6000 S4 Reagent Kit at Majorbio Bio-Pharm Technology Co., Ltd. (Shanghai, China). The data were analyzed on the free online platform of Majorbio Cloud Platform (www.majorbio.com). The best-hit taxonomy of non-redundant genes was obtained by aligning them against the NCBI NR database using DIAMOND[36] (http://ab.inf.uni-tuebingen.de/software/diamond/, version 2.0.11) with an e-value cut-off of 10^{-5}. Sequencing data including all field and incubated samples have been submitted to the NCBI Sequence Read Archive (accession No. SRP492072).

2.9. Histology and immunohistochemistry

Wound tissues were embedded in paraffin and sectioned at a thickness of 5 μm. Each section was stained with hematoxylin and eosin (H&E) for histological analysis and Masson's trichrome for collagen deposition. CD206/MRC1 (E6T5J) XP® Rabbit mAb (1:600, Abcam, Cambridge, UK), Proliferating Cell Nuclear Antigen (PCNA, (D3H8P) XP® Rabbit mAb (1:12000, Abcam, Cambridge, UK)) was used for immunohistochemistry (IHC) analysis. The proportion of positive cells was counted using Fiji ImageJ version 2.0 software (National Institutes of Health) by two independent researchers.

2.10. RNA isolation and quantitative real-time polymerase chain reaction

The wound tissues collected from the diabetic wound model, burn model, and GF wound model on Day 7 post-injury were used for RNA extraction. mRNA from wound tissues was extracted using Trizol reagent (Invitrogen, Carlsbad, CA, USA). Total mRNA (1 μg) was reverse-transcribed to complementary DNA using the SensiFAST cDNA synthesis kit (Bioline, London, US). Real-time PCR analysis was performed using SsoAdvanced Universal SYBR Green Supermix (Bio-Rad, Hercules, CA, USA). The efficiency of DNA amplification was evaluated using the mean cycle threshold (C_t) method. ΔC_t value was calculated from C_t values of different interest genes by subtracting the C_t value of the housekeeping gene, β-actin. The resulting relative mRNA expression was shown as fold change ($2^{-\Delta\Delta Ct}$) relative to the expression in baselines. The primer sequence (Sangon Biotech, Shanghai, China) is set as in Table 1.

2.11. Multi-plex analysis

The LX-MultiDTM-10 mouse cytokine assay (Bio-Rad, Hercules, CA, USA) was used to profile the expression of 10 inflammatory factors from terminal blood samples collected on Days 3 and 7 post-injury, including interleukin (IL)-1β, IL-2, IL-4, IL-5, IL-6, IL-10, IL-12p70, tumor necrosis factor-alpha (TNF-α), interferon-gamma (IFN-γ), and Chemokine (C-X-C motif) ligand 1 (CXCL1).

2.12. Collagen and synthetic monomers co-incubation with bacteria in vitro

Resuscitated *Escherichia coli* (*E. coli*, *ATCC25922*) and *Staphylococcus xylosus* (*S. xylosus*, *ATCC29971*) were cultured on Luria Bertani solid medium and sub-cultured in Luria Bertani liquid medium 12 h later, respectively. ε-Caprolactone [CL, 10 mg/mL, Shanghai Yuanye Biotechnology Co., Ltd. (Shanghai, China)], glycolic acid [GA, 10 mg/mL, Shanghai Yuanye Biotechnology Co., Ltd. (Shanghai, China)], and lactic acid [LA, 10 mg/mL, Shanghai Yuanye Biotechnology Co., Ltd. (Shanghai, China)], collagen [10 mg/mL, Solarbio (Beijing, China)], and collagen [0.8 mg/mL, Solarbio (Beijing, China)] were individually prepared in saline. A solution (1 mL) was then mixed with 1 mL of diluted bacterial solution respectively, while the NC group was mixed with 1 mL of saline, followed by cultivation at 37 °C. At each time point (0, 12, 24, 36, and 48 h), 100 μL was collected for analysis using an enzyme-labeled instrument.

2.13. Statistical analysis

The data were denoted as means ± standard error of mean (SEM) while all the statistical analyses were performed using the Graph Pad Prism software version 9.0 (GraphPad, ISI Software Inc., San Diego, CA, USA). Student's *t*-test analysis was utilized to determine significant differences between the two groups. One-way analysis of variance (ANOVA) was utilized to determine significant differences between multiple groups. $P < 0.05$ was considered statistical significance. ($^*P < 0.05$, $^{**}P < 0.01$, $^{***}P < 0.001$, $^{****}P < 0.0001$).

Table 1 The primer sequence (Sangon Biotech, Shanghai, China).

Gene	Primer	Sequence (5′-3′)
Actb	*Actb-F*	GGCTGTATTCCCCTCCATCG
	Actb-R	CCAGTTGGTAACAATGCCATGT
Mrc1	*Mrc1-F*	GTGGGGACCTGGCAAGTATC
	Mrc1-R	CACTGGGGTTCCATCACTCC
Arg1	*Arg1-F*	CTCCAAGCCAAAGTCCTTAGAG
	Arg1-R	GGAGCTGTCATTAGGGACATCA
Nos2	*Nos2-F*	GTTCTCAGCCCAACAATACAAGA
	Nos2-R	GTGGACGGGTCGATGTCAC
Tnf	*Tnf-F*	ATGGCCTCCCTCTCATCAGT
	Tnf-R	TTTGCTACGACGTGGGCTAC

3. Results

3.1. Synthetic scaffolds accelerated diabetic wound healing

In a typical experiment which is schematized in Fig. 1A, we first investigated the effects of natural and synthetic scaffolds within various biomaterials, external and internal structures on wound healing (Fig. 1B and C). All electrospun scaffolds and commercial dermal templates were characterized in terms of fiber width, pore size, and porosity (Fig. 1D, E and F). INT, MAD, PCL, and PLGA scaffolds were used to treat wounds in *db/db* mice (Fig. 2A) and the wound closure rate was measured on Days 3, 7, 14, and 21 among all the scaffolds. On Day 3, the results showed significantly faster wound closure for the animals receiving INT (28.0 ± 5.7%), PCL (18.4 ± 10.4%), and PLGA (27.8 ± 4.7%) compared to that of the NC group (−10.2 ± 5.5%), and MAD group (6.0 ± 8.2%). Next, on Day 7, both synthetic PCL and PLGA scaffolds had significantly faster wound closure of 50.1 ± 3.7% and 50.3 ± 4.4% compared to the NC group (17.1 ± 2.4%). The healing rate accounted for 36.4 ± 4.5% for INT and 22.1 ± 5.7% for MAD on Day 7. Meanwhile, the PCL group showed significantly faster wound closure compared to the MAD group. The synthetic PCL scaffold reached near-completed healing (98.7 ± 0.6%) on Day 14 while PLGA healed 90.8 ± 1.8%. In contrast, natural scaffolds of INT and MAD accounted for 73.9 ± 6.2% and 82.0 ± 5.9%, respectively. Finally, all wounds were reaching near-completed healing by Day 21 (Fig. 2B–D). H&E staining confirmed significantly faster re-epithelization in the PCL scaffold group (44.8 ± 4.2%) compared to NC (21.3 ± 3.2%), INT (21.6 ± 3.4%), MAD (18.2 ± 2.3%) groups on Day 7 (Fig. 2E and F). The surrounding tissue in both PCL and PLGA scaffold-treated wounds had flat skin with distinct layers of epidermis and dermis, although no hair follicles or skin appendages were noted. Moreover, re-epithelialization only appeared in the center of the wound bed in the PCL by Day 7. Masson's trichrome staining indicated low collagen deposition on Day 7 but on Day 21 within almost completely re-epithelization (Fig. 2G–I), the Masson's trichrome staining revealed that the PCL group (34.6 ± 7.7%) had significantly higher collagen density compared to the NC (9.4 ± 2.2%), INT (11.6 ± 1.2%), and MAD groups (10.4 ± 1.7%) (Fig. 2J). These results suggest that PCL scaffolds promote wound closure and stimulate increased collagen deposition in diabetic mice.

3.2. Natural and synthetic scaffolds reshaped diabetic wound microbiome

To examine the impact of natural and synthetic scaffolds on the wound microbiome, wound microbiome samples were then collected for 16S rRNA sequencing analysis. A-diversity shows the richness and evenness of the microbiome, and is evaluated using the Chao 1 index for the richness and the Shannon index for both the richness and evenness. β-Diversity reveals the differences in the composition of the microbiome among groups[35]. On Day 3, no significant differences were observed for both Chao 1 and Shannon indexes among all groups (Fig. 3A and B). However, on Day 7, the PCL group had a significantly higher Chao 1 index compared to those of the INT and MAD groups. In addition, the PCL group also showed a significantly higher

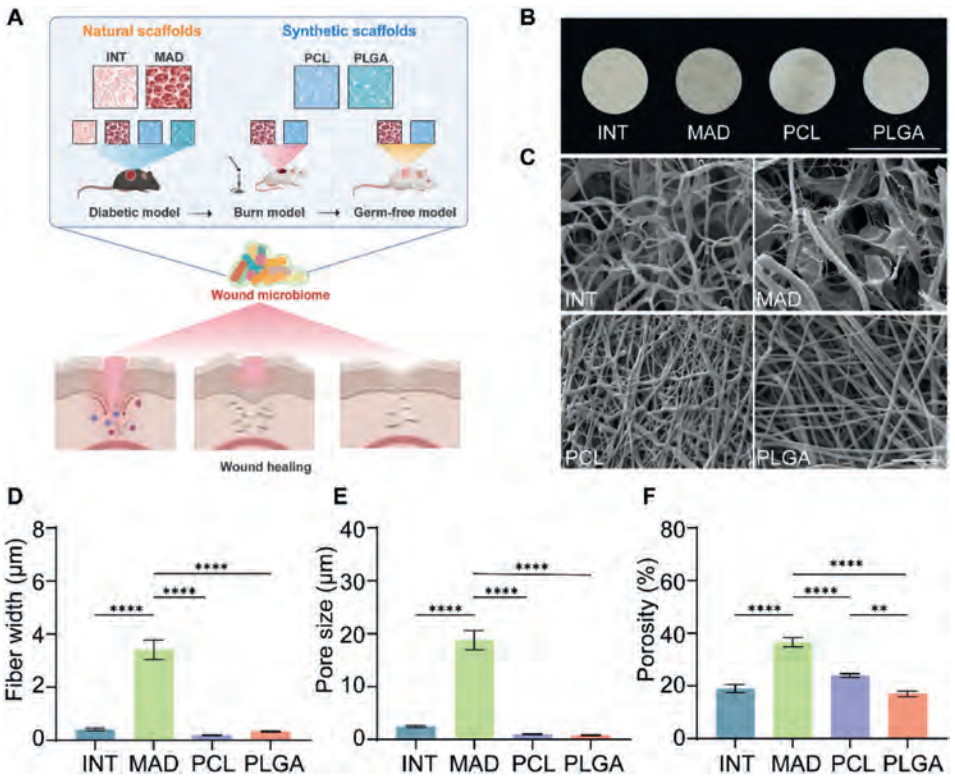

Figure 1 Schematic illustration and characterization of four scaffolds. (A) Schematic illustration. (B) Optical photographs of four scaffolds. Scale bars = 1 cm (white). (C) Scanning electron microscopy (SEM) images of four scaffolds. Scale bars = 5 μm (white). Fiber width (n = 30) (D), pore size (n = 10) (E), and porosity (n = 10) (F) of four scaffolds. $^{**}P < 0.01$, $^{****}P < 0.0001$. Data are presented as mean ± SEM.

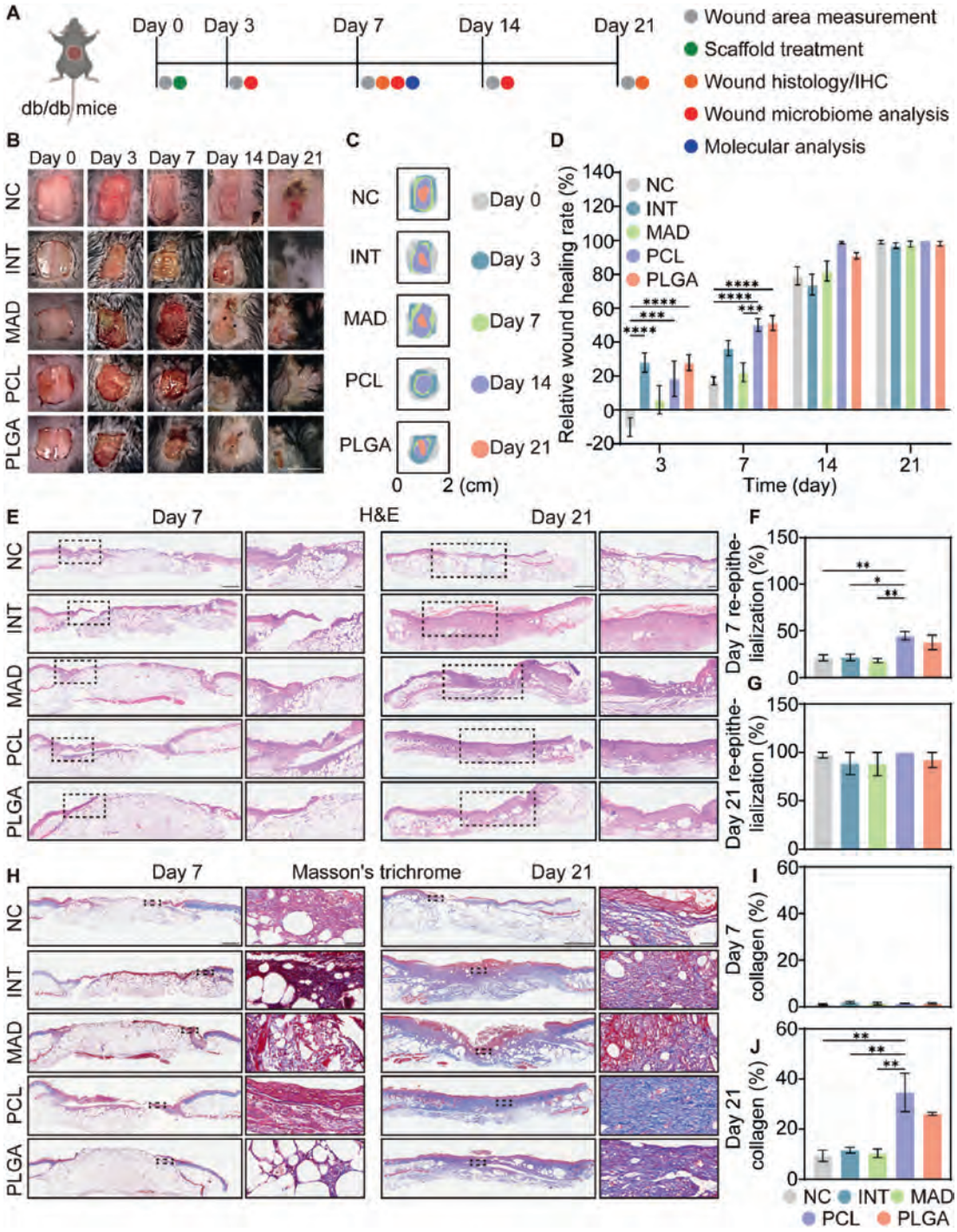

Figure 2 Natural and synthetic scaffolds-treated diabetic wound healing *in vivo*. (A) Schematic diagram of diabetic wound model. (B) Representative images of the diabetic wounds on Days 0, 3, 7, 14, and 21. Scale bar = 1 cm. (C) Traces of wound area for 21 days post-treatment. (D) Relative wound closure rate ($n = 5$). (E) H&E staining of wound tissues on Days 7 and 21. Scale bars: Day 7 = 1000 μm (left), 200 μm (right); Day 21 = 1000 μm (left), 200 μm (right). (F) Re-epithelialization of wounds on Day 7. (G) Re-epithelialization of wounds on Day 21. (H) Masson's trichrome staining of the wound bed on Days 7 and 21. Scale bars: Day 7 = 1000 μm (left), 200 μm (right); Day 21: Scale bars = 1000 μm (left), 50 μm (right). (I, J) Collagen deposition of wounds on Days 7 and 21. $^{*}P < 0.05$, $^{**}P < 0.01$, $^{***}P < 0.001$, $^{****}P < 0.0001$. Data are presented as mean ± SEM, $n = 3$.

Shannon index compared to the MAD group on both Days 7 and 14 (Fig. 3A and B). β-Diversity measured by PcoA showed that the composition and structure of the microbial community undergo significant changes after different scaffold treatments on Day 7 (Fig. 3C). The results from α-diversity and β-diversity suggested that Day 7 is a key time point in terms of changes in the wound microbiome. The Venn diagram showed that on Day 3, 9 OTUs were shared by all five groups, with 24, 66, 9, 3, and

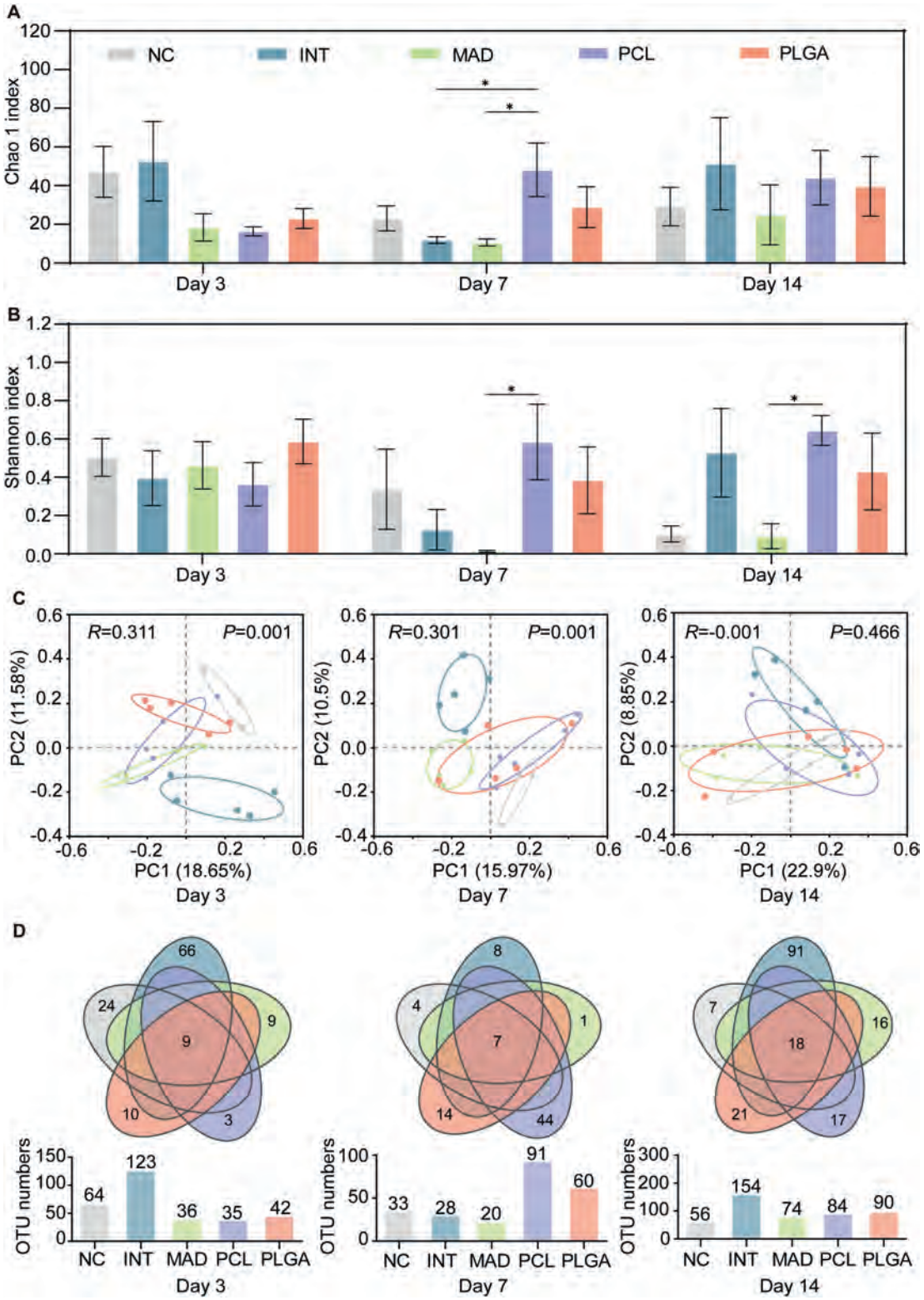

Figure 3 Analysis of the microbiome in diabetic wounds. (A) α-Diversity index based on Chao 1 on Days 3, 7, and 14 ($n = 3-5$). (B) α-Diversity index based on Shannon on Days 3, 7, and 14 ($n = 3-5$). (C) β-Diversity measured by PCoA on Days 3, 7, and 14 ($n = 3-5$). (D) Venn diagram on Days 3, 7, and 14 ($n = 3-5$). *$P < 0.05$. Data are presented as mean ± SEM, $n = 3-5$.

10 OTUs unique to NC, INT, MAD, PCL, and PLGA groups, respectively (Fig. 3D). On Day 7, 7 OTUs were shared by all five groups with 4, 8, 1, 44, and 14 OTUs unique to NC, INT, MAD, PCL, and PLGA groups, respectively. On Day 14, 18 OTUs were shared by all five groups, with 7, 91, 16, 17, and 21 OTUs unique to NC, INT, MAD, PCL, and PLGA groups, respectively. The Venn diagram containing all OTU levels is presented in Supporting Information (Supporting Information Fig. S1 A-C).

Next, the microbiome composition on the phylum level and genus level (the two main levels in microbiome composition analysis) were analyzed on Days 3, 7, and 14. On the phylum level, *Proteobacteria*, *Firmicutes*, and *Actinobacteriota* were identified as the predominant phyla across three time points (Fig. 4A−C). Further examination on the genus level revealed that *Escherichia*. *Shigella* (*E. Shigella*) and *Staphylococcus* were the two dominant microbiomes among the predominant phyla (Fig. 4D−F). As both α-diversity and β-diversity showed significant differences on Day 7, particularly between the MAD and PCL groups, MAD and PCL were selected for the following analysis. We analyzed the key microbiomes among NC, MAD and PCL groups on the phylum level and genus level. The relative abundance of key microbiomes on the phylum level was found to be *Proteobacteria* and *Firmicutes* as two key phyla on the phylum level (Fig. 4G). The genus-level analysis showed *E. Shigella* and *Staphylococcus* as key genera (Fig. 4H). *Citrobacter* was detected in the PCL group, but it does not show significant differences among the NC, MAD, and PCL groups. In the NC group, *Staphylococcus* accounted for 97.2%, 80.8% and 66.1% on Days 3, 7 and 14, consistent with a previous report showing *Staphylococcus* as the dominant microbiome in diabetic ulcers causing delayed healing[37]. Interestingly, 99.8% of the wound microbiome in the MAD group was found to be *E. Shigella* on Day 7. This finding may be the explanation for the poor repair of MAD treated diabetic mice. In the PCL group, *E. Shigella* were detected at 16.8%, 29.0% and 58.8%, while *Staphylococcus* was at 79.9%, 40.7% and 34.8% on Days 3, 7 and 14, respectively. This observation of a gradual increase in the abundance of *E. Shigella* in the PCL group from Day 3 to Day 14 (Fig. 4D−F), which may reversely inhibit the abundance of *Staphylococcus* and accelerate wound repair.

A metagenome analysis of the wound bacteria on Day 7 was further conducted for the most devised composition: *E. Shigella* and *Staphylococcus*. The results indicated that *E. coli* (*E. coli*) is the most dominant microbiome, accounting for 95.4%, 89.3%, and 93.9% in the NC, MAD, and PCL scaffolds on Day 7, respectively (Fig. 4I). In the *Staphylococcus* genus, *S. xylosus* (*S. xylosus*) is the most dominant microbiome in the NC group and PCL group, accounting for 85.7% and 82.7%, respectively (Fig. 4J). However, the dominant *Staphylococcus* genus found in the MAD-treated wounds was *Staphylococcus aureus*, accounting for 40.0% compared to 31.5% for *S. xylosus* (Fig. 4J). In diabetic wounds, MAD was identified as the least effective scaffold, while PCL scaffolds were determined to be the most effective scaffold.

3.3. Natural and synthetic scaffolds had comparable healing rates in burn injury mice

We extended our investigation to burn wounds, which is the most traumatic and physically debilitating injury that leads to significant morbidity and mortality. The effect of MAD and PCL scaffolds on burn wound repair in relation to the compositions of wound microbiomes was assessed (Fig. 5A). Wounds treated with MAD exhibited a higher tendency of healing rate on Day 7 compared to the NC and PCL groups (Fig. 5B−D). In the MAD group, wound closure was measured at 6.4 ± 8.2% on Day 3 and 37.8 ± 6.7% on Day 7. In contrast, the PCL scaffold demonstrated a slower healing rate of 1.9 ± 9.1% on Day 3 and 14.5 ± 9.8% on Day 7, while the NC group had the lowest healing rate of −13.1 ± 9.6% on Day 3 and 14.1 ± 5.1% on Day 7 (Fig. 5D). The MAD group also showed a higher tendency of re-epithelialization (Fig. 5E and F) but no significant differences. For the collagen deposition, the MAD group (26.8 ± 1.6%) had significantly higher collagen density than the NC (17.0 ± 0.7%), and PCL groups (15.7 ± 1.8%) (Fig. 5G and H) on Day 7.

The wound microbiome was collected for the 16S rRNA analysis. Neither α-diversity estimators nor β-diversity showed differences among the NC, MAD, and PCL groups (Fig. 5I−K), suggesting that natural and synthetic scaffolds appeared to have no effects on the diversity of the burn wound microbiome. The Venn diagram showed 46 OTUs shared by the three groups, with 87, 43, and 103 OTUs unique to the NC, MAD, and PCL groups, respectively (Fig. 5L). On the phylum level, the common microbiome detected in both burn and diabetic wounds included *Firmicutes* and *Proteobacteria* (Fig. 5M), with *Actinobacteria*, *Bacteroidota*, and *Cyanobacteria* identified as distinctive features in burn wounds (Fig. 5M). On the genus level, both burn and diabetic wounds contain *Staphylococcus*, with *Corynebacterium*, *Achromobacter*, *Enterobacter*, *Mammaliicocus*, *unclassified_F_Lachnospiraceae* and *unclassified_P_Cyanocharacter* unique to burn wounds (Fig. 5N). Interestingly, the burn wounds are lack of *E. Shigella* (Fig. 5N) and the changes in the composition of the wound microbiome may explain the comparable healing rates observed in burn injury wounds treated with MAD and PCL in contrast to those in diabetic wounds.

3.4. Natural scaffold, MAD significantly accelerated wound healing in GF mice

To further explore whether the response of the wound microbiome to natural and synthetic scaffolds plays a key role in wound repair, we employed a germ-free (GF) wound healing model (Fig. 6A). Microscopic examination results confirmed the presence of bacteria in SPF mice, while no bacteria were found in GF mice (Supporting Information Fig. S2). In the results, MAD exhibited a healing rate of approximately 4.6 ± 8.7% on Day 3, contrasting with the 2.1 ± 4.9% and −2.5 ± 11.5% observed in the NC and PCL groups, respectively. On Day 7, the healing rate of the MAD group (50.4 ± 3.7%) was significantly higher than that of the NC group (28.9 ± 4.0%) and faster than the PCL group (36.7 ± 4.3%) (Fig. 6B−D). This data suggested that in GF mice without bacteria, the healing rates of the MAD and PCL groups have opposite tendencies compared to those observed in the diabetic wounds. H&E staining further confirmed a significantly accelerated re-epithelialization of wounds treated with MAD in the GF animals (Fig. 6E and F). On Day 7, re-epithelialization of 52.1 ± 6.1% occurred in the MAD group compared to 17.1 ± 2.7% and 29.9 ± 4.0% in the NC and PCL groups, respectively. Masson's trichrome staining showed a notably higher collagen density of 17.4 ± 2.1% in the MAD group (Fig. 6G and H), contrasting with 9.3 ± 0.8% in the PCL group and 7.4 ± 1.2% in the NC group. The result of PCNA staining of proliferative cells showed that MAD has the most positively stained $PCNA^+$ cells (13.5 ± 0.6%) and is significantly higher than NC (4.3 ± 0.6%) and PCL (6.5 ± 1.6%) groups (Fig. 6I and J). This may be explained by the release of collagen from MAD scaffolds to promote cell proliferation, thereby accelerating wound healing in the MAD group when the microbiome was fully eliminated.

3.5. Collagen stimulates E. coli growth in vitro

To investigate whether natural scaffolds stimulate the rapid growth of bacteria, particularly *E. coli*, at the wound site during diabetic wound healing, we conducted *in vitro* co-incubation experiments. Collagen, the major components of MAD and INT and monomers

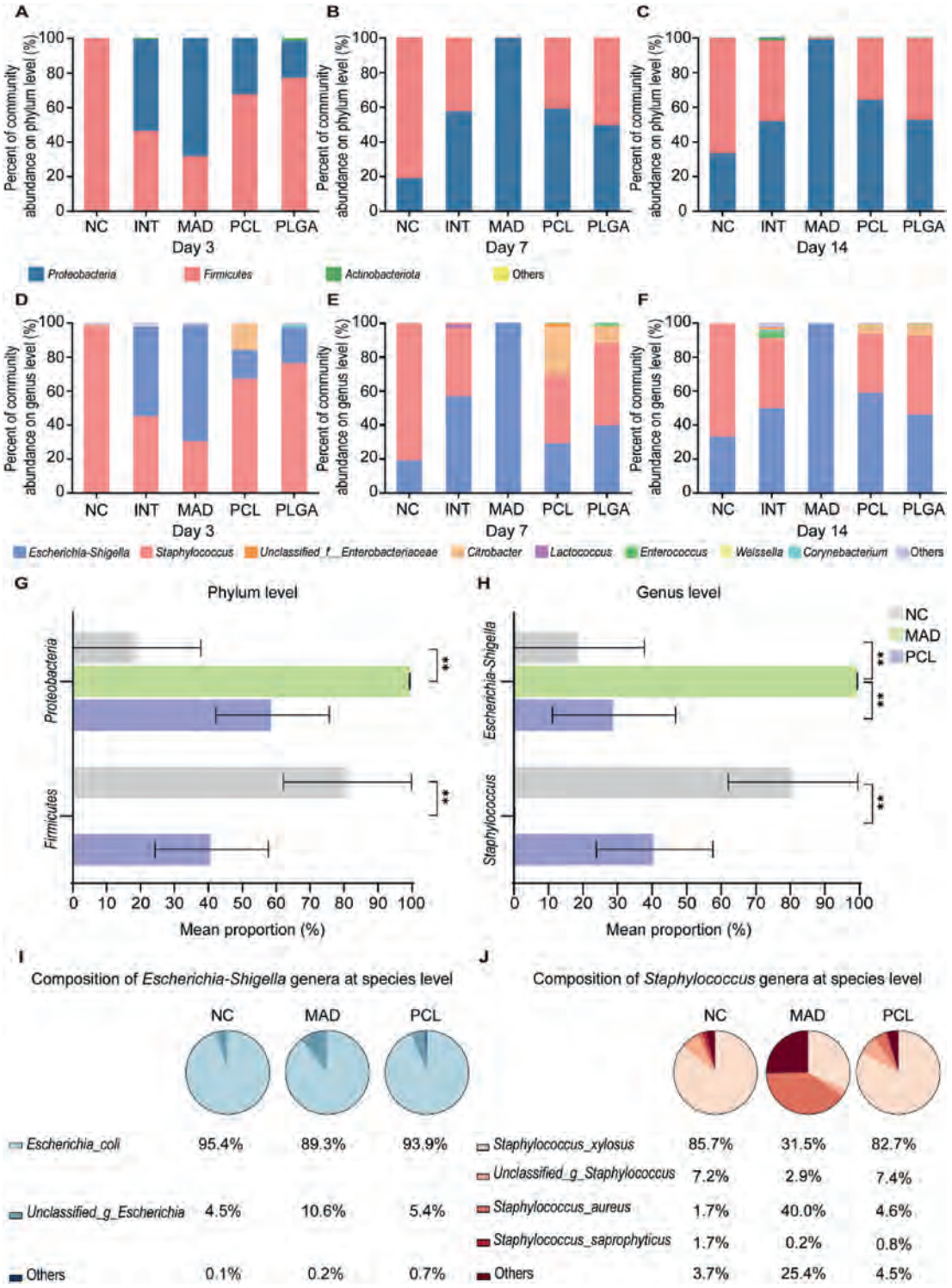

Figure 4 Diabetic wound microbiome analysis. (A–C) Percentage of community composition on the phylum level on Days 3, 7, and 14 (n = 3–5). (D–F) Percentage of community composition on the genus level on Days 3, 7, and 14 (n = 3–5). (*Unclassified_F_Enterobacteriaceae* means a microbiome on the genus level, but its name is not included in the database and can only be determined on the family level of Enterobacteriaceae). (G) Relative abundance of key microbiomes on the phylum level (n = 3–5). (H) Relative abundance of key microbiomes on the genus level (n = 3–5). (I) Composition of *Escherichia-Shigella* by metagenome analysis on Day 7 (n = 3–5). (J) Composition of *Staphylococcus* by metagenome analysis on Day 7 (n = 3–5). $^{**}P < 0.01$. Data are presented as mean ± SEM, n = 3–5.

including CL, GA, and LA, the major components of PCL and PLGA scaffolds, were co-incubated with *E. coli* or *S. xylosus* (Fig. 7A and B). The results revealed that synthetic monomers CL, GA, and LA, at a concentration of 10 mg/mL, had an inhibitory effect on the growth of *E. coli*, showing lower absorbance compared to the NC. In contrast, collagen (10 mg/mL)

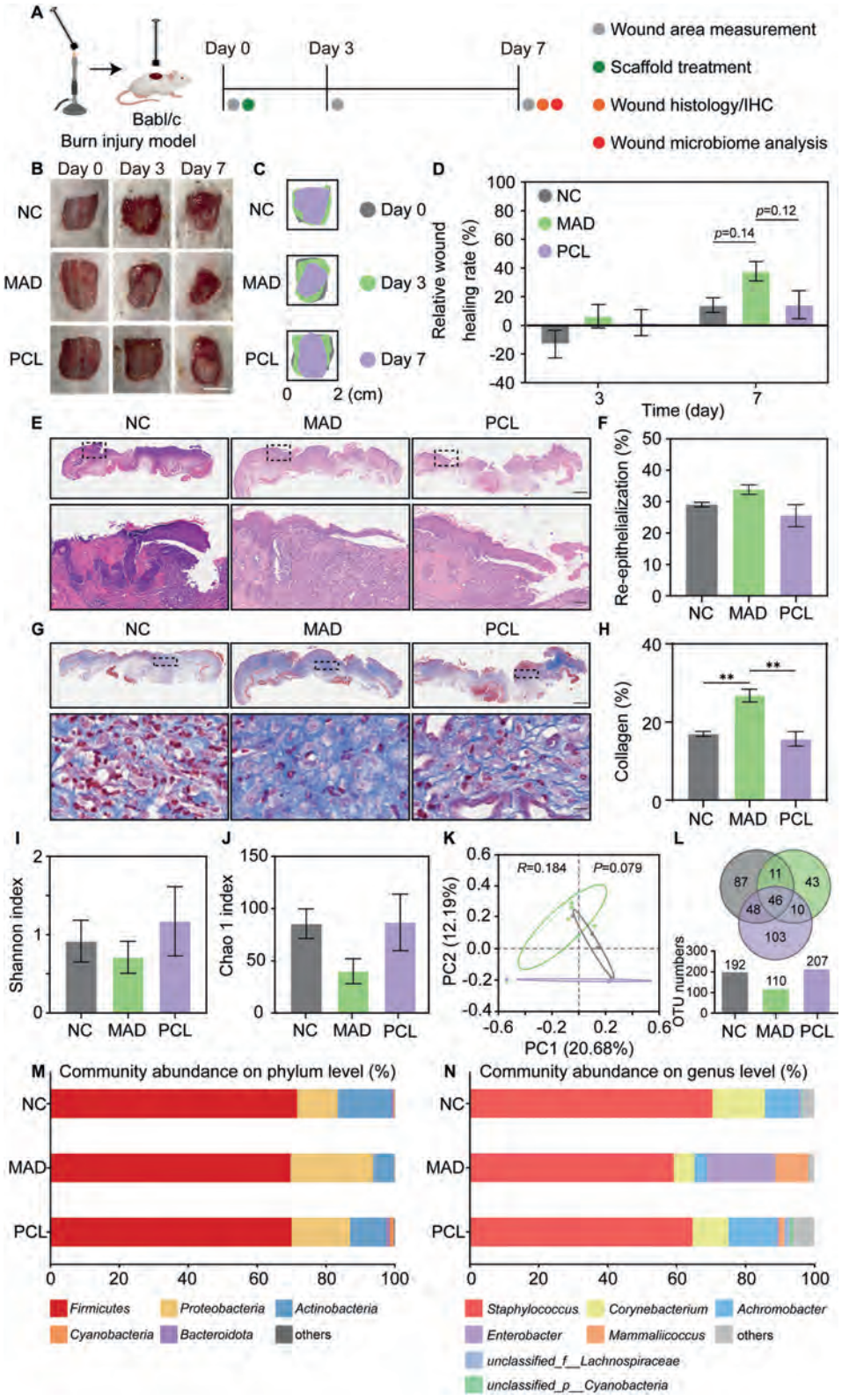

Figure 5 MAD and PCL scaffolds-treated burn wound healing *in vivo*. (A) Schematic diagram of burn wound model. (B) Representative digital images of the burn wounds on Days 0, 3, and 7. Scale bar = 1 cm. (C) Traces of the wound over 7 days for each treatment. (D) Relative wound healing rate (n = 4−5). (E) H&E staining of wounds on Day 7. Scale bars = 1000 μm (Above), 80 μm (Below). (F) Re-epithelialization on Day 7 (n = 3). (G) Masson's trichrome staining on Day 7. Scale bars = 1000 μm (Above), 10 μm (Below). (H) Collagen deposition on Day 7. (I, J) Shannon index and Chao 1 index on the OTU level on Day 7 (n = 4−5). (K) β-diversity measured by PCoA (n = 4−5) and (L) Venn diagram on Day 7 (n = 4−5). (M) Community abundance on the phylum level (n = 4−5) and (N) community abundance on the genus level on Day 7

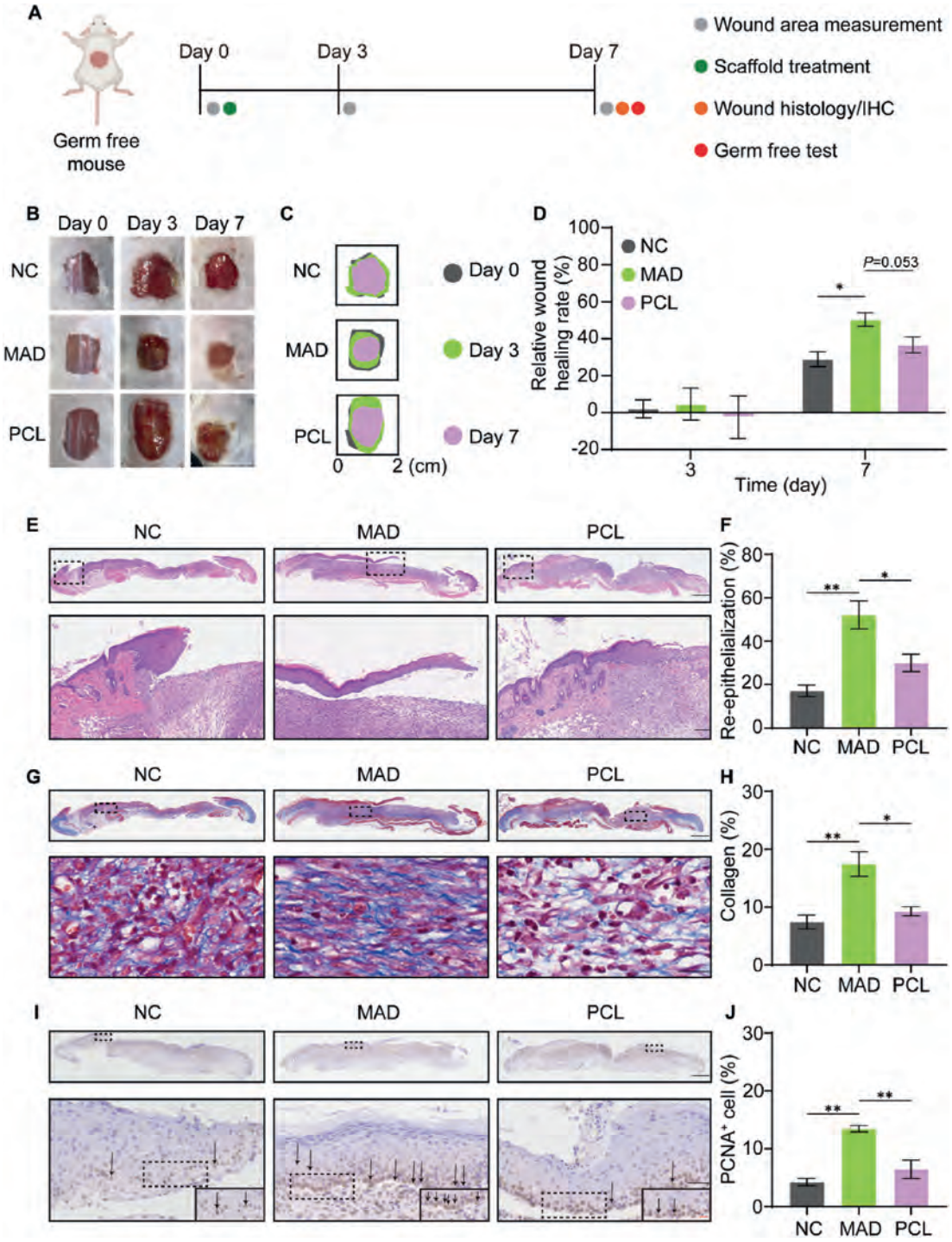

Figure 6 MAD and PCL scaffolds-treated GF wound healing *in vivo*. (A) Schematic diagram of GF wound model. (B) Representative digital images of the GF wounds on Days 0, 3, and 7. Scale bar = 1 cm. (C) Traces of wound over 7 days for each treatment. (D) Relative wound healing rate ($n = 4$). (E) H&E staining of wounds on Day 7. Scale bars = 1000 μm (above), 120 μm (below). (F) Re-epithelialization on Day 7. (G) Masson's trichrome staining on Day 7. Scale bars = 1000 μm (above), 20 μm (below). (H) Collagen deposition on Day 7. (I) Images of immunohistochemical staining of PCNA on Day 7. Scale bars = 1000 μm (above), 50 μm (below), 20 μm (red). (J) Quantitative analysis of $PCNA^+$ cells on Day 7. $^*P < 0.05$, $^{**}P < 0.01$. Data are presented as mean ± SEM.

($n = 4$–5). (*Unclassified_F_Lachnospiraceae* or *Unclassified_P_Cyanocharacter* means a microbiome on the genus level, but its name is not included in the database and can only be determined on the phylum level of *Lachnospiraceae* or *Cyanocharacter*, respectively). $^{**}P < 0.01$. Data are presented as mean ± SEM.

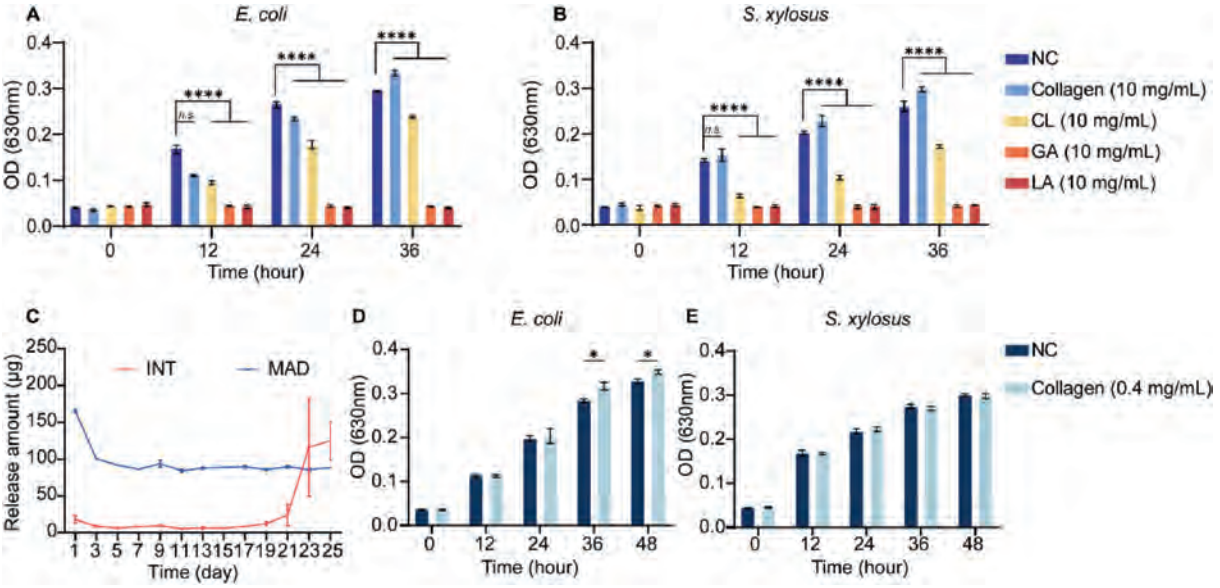

Figure 7 (A) *In vitro* co-incubation of collagen and different monomers (10 mg/mL) with *E. coli* and (B) *S. xylosus*. (C) *In vitro* release of collagen from INT and MAD. (D) 0.4 mg/mL collagen co-incubated with *E. coli* and (E) *S. xylosus in vitro*. *$P < 0.05$, ****$P < 0.0001$. *n.s.*, not significant. Data are presented as mean ± SEM, $n = 3$.

demonstrated significantly faster growth of *E. coli* compared to the NC. A similar trend was also observed when these monomers were co-incubated with *S. xylosus,* with collagen also stimulating *S. xylosus* growth. This data suggests that collagen released from natural scaffolds regulates the wound microbiome.

To further explore this hypothesis, we conducted an *in vitro* collagen release study from INT and MAD in PBS at 37 °C (Fig. 7C). INT scaffolds exhibited a slow release at approximately 20 μg/mL/day until Day 23, followed by a burst release at 115 μg/mL/day thereafter. This gradual release is attributed to the cross-linking of INT using glutaraldehyde[38]. In contrast, non-crosslinked MAD scaffolds showed a rapid release of approximately 165 μg on Day 1 followed by 100 μg/mL/day in PBS at 37 °C, potentially contributing to the excessive proliferation of *E. coli* at the diabetic wound site evidenced by over 99% detection from 16S rRNA sequencing analysis. The cumulative release of collagen from MAD in 7 days was measured to be approximately 400 μg. Subsequently, we performed *in vitro* co-incubation experiments using collagen at a concentration of 400 μg/mL. Collagen at this concentration promoted the proliferation of *E. coli* but had no effect on *S. xylosus* (Fig. 7D and E), confirming that the faster release of collagen from MAD could be the reason for the rapid growth of *E. coli* and delayed wound healing in diabetic mice.

3.6. Microbiome regulated inflammation in diabetic healing model

Natural and synthetic scaffolds were found to regulate the wound microbiome, particularly in diabetic wound repair. To further explore whether changes in the wound microbiome influence inflammation, the protein expression of pro-inflammatory factors (IFN-γ, IL-6, IL-1β, TNF-α, IL-5, IL-2, IL-12p70) and anti-inflammatory factors (IL-10, IL-4), along with the chemokine CXCL1, were examined at the serum level on Days 3 and 7 (Supporting Information Figs. S3A and S3B). The mRNA expression of pro-inflammatory factors (*Tnf*,*Nos2*) and anti-inflammatory factors (*Arg1*, *Mrc1*) on Day 7 was also examined at the tissue level (Fig. 8A−D and G) in the diverse wound healing models among the NC, MAD, and PCL groups.

In the diabetic model, the results showed no significant differences in inflammation biomarkers at the serum level. The mRNA expression of pro-inflammatory factor *Tnf* was found significantly higher in the MAD group compared to the PCL and NC groups (Fig. 8A). Conversely, PCL scaffolds stimulated a significantly high expression of anti-inflammatory factors, specifically *Mrc1* levels compared to the MAD group (Fig. 8A). IHC staining confirmed higher CD206 expression in the PCL group (Fig. 8B and C), suggesting that in the diabetes model, PCL scaffolds modulate the wound microbiome, leading to an upregulation of anti-inflammation together with accelerated diabetic wound repair. In the burn injury model, there were no significant differences at mRNA expression among MAD, PCL, and NC groups (Fig. 8D). IHC results confirmed changes in inflammation, while no changes were noted for CD206 staining (Fig. 8E and F). For the GF mice, the NC group exhibited an exceptionally low inflammatory response, typical of sterile wounds that elicit a mild immune reaction[39]. Upon the application of MAD and PCL scaffolds on the wound site, both scaffolds induced inflammation. However, no significant differences were observed between MAD and PCL (Fig. 8G−I).

4. Discussion

In the clinical management of wounds, dermal templates and skin substitutes are utilized to promote wound repair. Additionally, various novel scaffolds are being developed to regulate the inflammatory response and microenvironments, and enhance neo-vascularization, and cell proliferation[5-7]. However, the regulation of the wound microbiome by different templates and scaffolds has not been investigated and seems to be overlooked in the healing process. In this study, we demonstrate that synthetic scaffolds, including PCL and

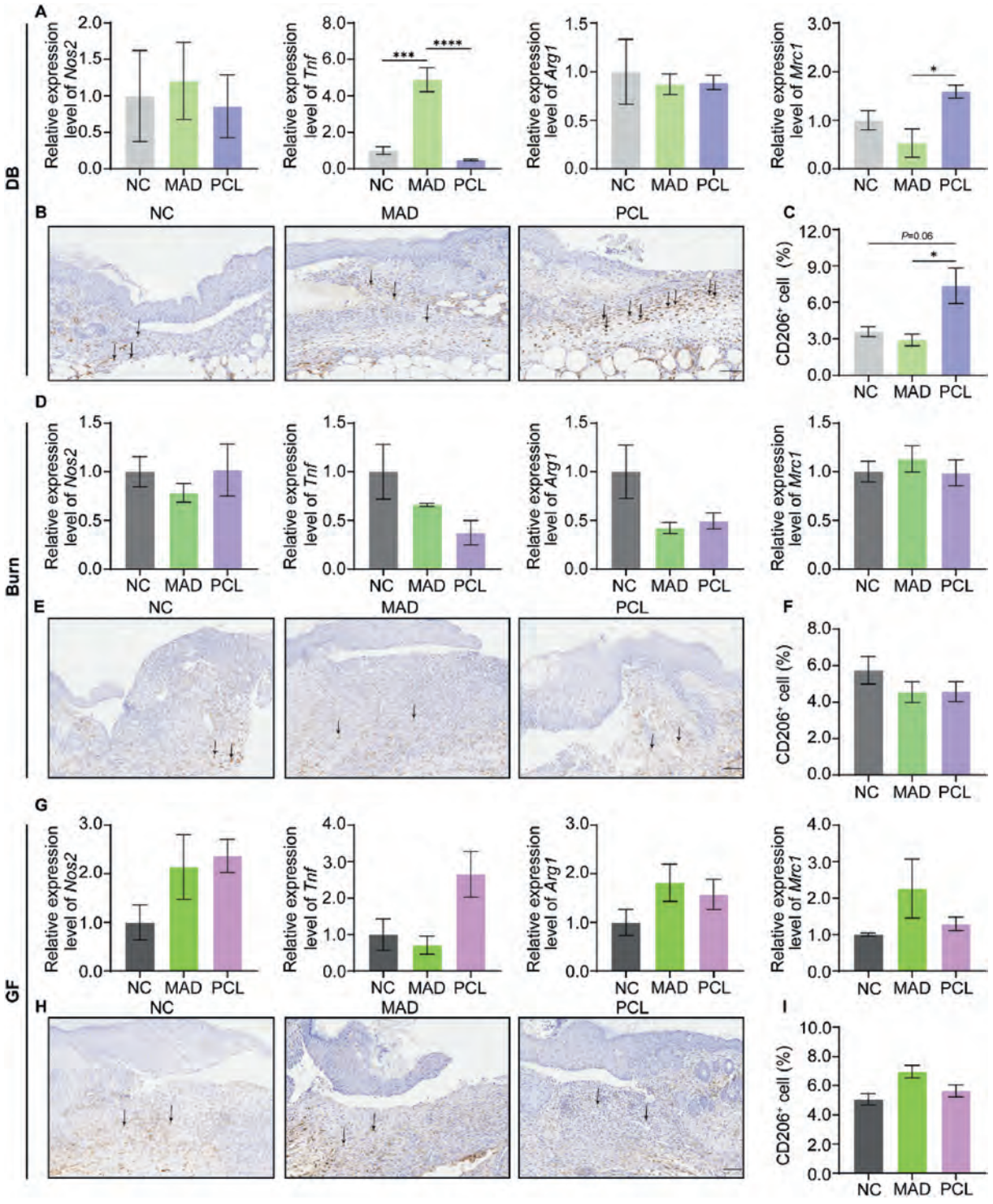

Figure 8 Inflammation analysis. (A) The mRNA expression of *Nos2*, *Tnf*, *Arg1*, and *Mrc1* on Day 7 in the diabetic wound. (B) Immunohistochemical staining of CD206 on Day 7 in the diabetic wound. Scale bars = 100 μm. (C) Quantitative analysis of $CD206^+$ IHC staining in the diabetic wound. (D) The mRNA expression of *Nos2*, *Tnf*, *Arg1*, and *Mrc1* on Day 7 in the burn wound. (E) Immunohistochemical staining of CD206 on Day 7 in burn wound. Scale bars = 100 μm. (F) Quantitative analysis of $CD206^+$ IHC staining in the burn wound. (G) The mRNA expression of *Nos2*, *Tnf*, *Arg1*, and *Mrc1* on Day 7 in the GF wound. (H) Immunohistochemical staining of CD206 on Day 7 in GF wound. Scale bars = 100 μm. (I) Quantitative analysis of $CD206^+$ IHC staining in the GF wound. $^*P < 0.05$, $^{***}P < 0.001$, $^{****}P < 0.0001$. Data are presented as mean ± SEM, $n = 3$.

PLGA scaffolds, significantly enhance the healing of diabetic wounds compared to natural dermal templates such as INT and MAD. Moreover, analysis of 16S rRNA data further reveals that the composition of wound microbiomes was greatly influenced by different types of scaffolds. Notably, PCL scaffolds contribute to the enrichment and diversity of the wound microbiome. Diverse microbiomes have been shown to provide health benefits by resisting pathogen colonization[40]. Furthermore, a clinical study reported that the diversity of the wound microbiome in patients with diabetic ulcers is lower than in healthy individuals, potentially contributing to the challenge of non-healing wounds[41]. Our data show that a more diverse microbiome regulated by PCL scaffolds may be crucial to promoting diabetic wound healing. In contrast, the colonization of 99% *E.coli* in the MAD group was identified as a risk factor causing a significant delay in diabetic wound healing. This observation aligns with a clinical report indicating that a higher incidence of wound infectious complications are associated with the use of natural templates[42]. The colonization of pathogenic *Staphylococcus* was reported to negatively affect diabetic wound healing[21], due to disruptions of the homeostasis of the skin microbiome[17-19]. The application of synthetic scaffolds in the diabetic wounds was found to decrease the proportion of *Staphylococcus*, accompanied by an increasing trend in the proportion of *E. Shigella*. This protective effect of a single strain with enhanced community diversity is consistent with a recent report on the gut microbiome, showing community-level resistance rested critically upon certain species being present[40].

To better understand how natural and synthetic scaffolds impact the microbiome of burn injuries, we utilized MAD and PCL scaffolds in the process of burn wound healing. Previous studies have identified *Pseudomonas* and *Staphylococcus* as microbiome in burn wounds for both humans and rodents[43]. However, our 16S rRNA analysis revealed the absence of *E. Shigella* in all groups with the burn injury. Notably, despite the absence of *E. Shigella* in burn wounds, both natural (MAD) and synthetic (PCL) scaffolds exhibited comparable rates of burn wound healing. We then used the GF wound model to further investigate the influence of commensal wound microbiome on wound repair treated with natural and synthetic scaffolds. Data revealed a reversed outcome, indicating that MAD significantly accelerated wound healing in GF mice by Day 7 compared to synthetic PCL scaffolds. These findings substantiate the notion that the wound microbiome, influenced by distinct scaffolds, plays a crucial role in wound repair. Overall, the findings are consistent with clinical practices. Generally, wounds in diabetic patients are often colonized by pathogens. These wounds are required to be debrided prior to the application of dermal templates, particularly the natural scaffolds as they can increase the risk of wound infections.

Furthermore, this study emphasizes that the colonization of *E. Shigella* can be protective only when in combination with other wound microbiomes, but an over-proliferation of *E. Shigella* negatively impacts diabetic wound healing. We then investigated whether released collagen or monomers from various scaffolds regulate microbiome communities. Co-culturing collagen or CL, LA, GA, with *S. xylosus* or *E. coli*., showed that collagen can promote both *S. xylosus* and *E. coli* growth at the highest soluble concentration but only stimulated *E. coli* growth at the released concentration from MAD scaffolds *in vitro*. This discovery suggests that sustained delivery of collagen from non-crosslinked natural scaffolds may pose a significant risk in the clinical treatment of diabetic ulcers, especially for patients with commensal *E. coli* present at the wound site. The synthetic monomers, CL, GA and LA, had minimal effects on the microbiome, confirming that the changes of wound microbiomes in the diabetic model is due to scaffolds rather than monomers.

The wound microbiome is reported to mediate inflammation[44,45]. Overexpression of pro-inflammatory cytokines and proteases, along with reduced growth factors, is known to delay healing due to macrophage dysfunction. Macrophages play an essential role in mediating inflammatory response post-injury. M1 macrophages dominate pro-inflammatory factors such as *Nos2*, *Tnf*, *Il6*, while M2 macrophages with anti-inflammatory effects secrete *Arg1*, *Mrc1*, *Il10* and attenuate inflammation. A recent study showed that the wound microbiome can activate neutrophils to express chemokine CXC ligand 10, enhancing dendritic cell recruitment and subsequently stimulating fibroblasts and macrophages to promote wound healing[45]. Another study found that the microbiome reversed the turn-over of inflammation by transforming M1 macrophages into M2 macrophages[46]. These findings suggest that wound microbiome's regulation of macrophage polarization is highly involved in inflammation, thereby resulting in improved wound repair. In our study of the diabetic model, following MAD treatment, the mRNA levels of pro-inflammatory biomarker: *Tnf* was found to be significantly higher compared to those in the PCL group, indicating that the rapid proliferation of *E. coli* as well as faster collagen released from MAD stimulate a prolonged inflammatory response. This may contribute to M1 macrophage recruitment with extensive secretion of pro-inflammatory factors[47]. Conversely, the anti-inflammatory biomarker *Mrc1* was notably higher in the PCL group. This may be attributed to the increased percentage of *E. coli*, along with enhanced diversity of wound microbiome, resulting in elevated anti-inflammatory response and promoted wound healing. Similar results were observed when M2 macrophage ratio increased through modification of the wound microbiome in diabetic animals[48]. In the burn injury model, no significant differences in inflammatory biomarkers were observed between natural and synthetic scaffolds. The lack of such a difference may be attributed to the absence of *E. coli* in the burn model, resulting in a similar inflammatory response in burn injuries. Moreover, GF mice, which lack of bacteria, exhibited extremely low inflammation post-injury compared to other two models in the NC groups, while the inflammatory response was triggered by scaffolds only.

5. Conclusions

In summary, our study investigated the impacts of natural and synthetic scaffolds on the wound microbiome across various wound healing models. Our findings demonstrate over-growth of *E. coli* stimulated by collagen released from biological scaffolds, impedes the repair of diabetic wounds. Conversely, synthetic scaffolds promoted a more diverse wound microbiome which exhibited a protective effect and faster healing process of diabetic wounds. The reconstruction of the wound microbiome in response to both types of scaffolds appears pivotal in regulating inflammation. Understanding the influence of scaffold-regulated wound microbiomes could significantly contribute to the future design and development of dermal templates and skin substitutes.

Acknowledgments

We are grateful to the National Natural Science Foundation of China (No. 82372521, 82172217, 82104110, 82003305), the Natural Science Foundation of Jiangsu Province (No. BK20210691, China), the Natural Science Foundation of Nanjing

University of Chinese Medicine (XZR2023071, XPT82104110, China).

Author contributions

Zeyu Xu: Writing − review & editing, Writing − original draft, Visualization, Methodology, Investigation, Conceptualization. Lixiang Zhang: Methodology, Investigation. Qinghan Tang: Methodology, Investigation. Chenxi Yang: Methodology, Investigation. Xiaotong Ding: Methodology, Investigation. Ziyu Wang: Visualization. Rizhong Huang: Validation. Ruihan Jiang: Validation. Joannake Maitz: Supervision. Huaikai Shi: Supervision. Xin Yan: Supervision. Mei Dong: Writing − review & editing, Visualization, Conceptualization. Jun Chen: Writing − review & editing, Funding acquisition, Conceptualization. Yiwei Wang: Writing − review & editing, Writing − original draft, Supervision, Funding acquisition, Conceptualization.

Conflicts of interest

The authors have no conflicts of interest to declare.

Appendix A. Supporting information

Supporting information to this article can be found online at https://doi.org/10.1016/j.apsb.2024.08.024.

References

1. Tomic-Canic M, Burgess JL, O'Neill KE, Strbo N, Pastar I. Skin microbiota and its interplay with wound healing. *Am J Clin Dermatol* 2020;**21**:36−43.
2. Kalan LR, Brennan MB. The role of the microbiome in nonhealing diabetic wounds. *Ann N Y Acad Sci* 2019;**1435**:79−92.
3. Jeschke MG, van Baar ME, Choudhry MA, Chung KK, Gibran NS, Logsetty S. Burn injury. *Nat Rev Dis Primers* 2020;**6**:11.
4. Chen L, Li ZY, Zheng YT, Zhou F, Zhao JL, Zhai QY, et al. 3D-printed dermis-specific extracellular matrix mitigates scar contraction via inducing early angiogenesis and macrophage M2 polarization. *Bioact Mater* 2022;**10**:236−46.
5. Zhang J, Luo Q, Hu Q, Zhang T, Shi J, Kong L, et al. An injectable bioactive dressing based on platelet-rich plasma and nanoclay: sustained release of deferoxamine to accelerate chronic wound healing. *Acta Pharm Sin B* 2023;**13**:4318−36.
6. Wang Y, Lv Q, Chen Y, Xu L, Feng M, Xiong Z, et al. Bilayer hydrogel dressing with lysozyme-enhanced photothermal therapy for biofilm eradication and accelerated chronic wound repair. *Acta Pharm Sin B* 2023;**13**:284−97.
7. Liu Y, Zhuang B, Yuan B, Zhang H, Li J, Wang W, et al. Predatory bacterial hydrogels for topical treatment of infected wounds. *Acta Pharm Sin B* 2023;**13**:315−26.
8. Chua AWC, Khoo YC, Tan BK, Tan KC, Foo CL, Chong SJ. Skin tissue engineering advances in severe burns: review and therapeutic applications. *Burns Trauma* 2016;**4**:3.
9. Mahmood A, Patel D, Hickson B, DesRochers J, Hu X. Recent progress in biopolymer-based hydrogel materials for biomedical applications. *Int J Mol Sci* 2022;**23**:1415.
10. Kawai K, Suzuki S, Tabata Y, Ikada Y, Nishimura Y. Accelerated tissue regeneration through incorporation of basic fibroblast growth factor-impregnated gelatin microspheres into artificial dermis. *Biomaterials* 2000;**21**:489−99.
11. Anilkumar TV, Muhamed J, Jose A, Jyothi A, Mohanan PV, Krishnan LK. Advantages of hyaluronic acid as a component of fibrin sheet for care of acute wound. *Biologicals* 2011;**39**:81−8.
12. Yamamoto M, Ikada Y, Tabata Y. Controlled release of growth factors based on biodegradation of gelatin hydrogel. *J Biomat Sci-polym E* 2001;**12**:77−88.
13. Slavkovsky R, Kohlerova R, Jiroutova A, Hajzlerova M, Sobotka L, Cermakova E, et al. Effects of hyaluronan and iodine on wound contraction and granulation tissue formation in rat skin wounds. *Clin Exp Dermatol* 2010;**35**:373−9.
14. Gao F, Liu YW, He YQ, Yang CX, Wang YZ, Shi XX, et al. Hyaluronan oligosaccharides promote excisional wound healing through enhanced angiogenesis. *Matrix Biol* 2010;**29**:107−16.
15. Wang YW, Beekman J, Hew J, Jackson S, Issler-Fisher AC, Parungao R, et al. Burn injury: challenges and advances in burn wound healing, infection, pain and scarring. *Adv Drug Deliv Rev* 2018;**123**:3−17.
16. Chaudhari AA, Vig K, Baganizi DR, Sahu R, Dixit S, Dennis V, et al. Future prospects for scaffolding methods and biomaterials in skin tissue engineering: a review. *Int J Mol Sci* 2016;**17**:1974.
17. Chen YE, Fischbach MA, Belkaid Y. Skin microbiota-host interactions. *Nature* 2018;**553**:427−36.
18. Belkaid Y, Segre JA. Dialogue between skin microbiota and immunity. *Science* 2014;**346**:954−9.
19. Harris-Tryon TA, Grice EA. Microbiota and maintenance of skin barrier function. *Science* 2022;**376**:940−5.
20. Kalan LR, Meisel JS, Loesche MA, Horwinski J, Soaita I, Chen XX, et al. Strain- and species-level variation in the microbiome of diabetic wounds is associated with clinical outcomes and therapeutic efficacy. *Cell Host Microbe* 2019;**25**. 641-55.e5.
21. Chuan FN, Tang K, Jiang P, Zhou B, He XQ. Reliability and validity of the perfusion, extent, depth, infection and sensation (PEDIS) classification system and score in patients with diabetic foot ulcer. *PLoS One* 2015;**10**:e0124739.
22. Wang GF, Sweren E, Liu HY, Wier E, Alphonse MP, Chen RS, et al. Bacteria induce skin regeneration via IL-1β signaling. *Cell Host Microbe* 2021;**29**:777−791.e6.
23. Armstrong DG, Tan TW, Boulton AJM, Bus SA. Diabetic foot ulcers: a review. *Jama* 2023;**330**:62−75.
24. Lousada MB, Lachnit T, Edelkamp J, Rouillé T, Ajdic D, Uchida Y, et al. Exploring the human hair follicle microbiome. *Br J Dermatol* 2021;**184**:802−15.
25. Muraoka WT, Granados JC, Gomez BI, Nicholson SE, Chung KK, Shupp JW, et al. Burn resuscitation strategy influences the gut microbiota-liver axis in swine. *Sci Rep* 2020;**10**:15655.
26. Uberoi A, McCready-Vangi A, Grice EA. The wound microbiota: microbial mechanisms of impaired wound healing and infection. *Nat Rev Microbiol* 2024;**22**:507−21.
27. Tang QH, Xue NN, Ding XF, Tsai KHY, Hew JJ, Jiang RH, et al. Role of wound microbiome, strategies of microbiota delivery system and clinical management. *Adv Drug Deliv Rev* 2023;**192**:114671.
28. Chen SL, Lundy DJ, Ruan SC, Chen HC, Chao YK, Cheng YY, et al. The gut microbiota regulates acute foreign body reaction and tissue repair after biomaterial implantation. *Biomaterials* 2022;**289**:121807.
29. Shi HK, Tsai KHY, Ma DC, Wang XS, Desai R, Parungao RJ, et al. Controlled dual release of dihydrotestosterone and flutamide from polycaprolactone electrospun scaffolds accelerate burn wound healing. *FASEB J* 2022;**36**:e22310.
30. Rnjak-Kovacina J, Weiss AS. Increasing the pore size of electrospun scaffolds. *Tissue Eng B-re* 2011;**17**:365−72.
31. Hew JJ, Parungao RJ, Shi HK, Tsai KHY, Kim S, Ma DC, et al. Mouse models in burns research: characterisation of the hypermetabolic response to burn injury. *Burns* 2020;**46**:663−74.
32. Chen SF, Zhou YQ, Chen YR, Gu J. Fastp: an ultra-fast all-in-one FASTQ preprocessor. *Bioinformatics* 2018;**34**:i884−90.
33. Magoc T, Salzberg SL. FLASH: fast length adjustment of short reads to improve genome assemblies. *Bioinformatics* 2011;**27**:2957−63.
34. Edgar RC. UPARSE: highly accurate OTU sequences from microbial amplicon reads. *Nat Methods* 2013;**10**:996−8.
35. Qian XB, Chen T, Xu YP, Chen L, Sun FX, Lu MP, et al. A guide to human microbiome research: study design, sample collection, and bioinformatics analysis. *Chin Med J Engl* 2020;**133**:1844−55.

36. Buchfink B, Xie C, Huson DH. Fast and sensitive protein alignment using DIAMOND. *Nat Methods* 2015;**12**:59−60.
37. Dryden M, Baguneid M, Eckmann C, Corman S, Stephens J, Solem C, et al. Pathophysiology and burden of infection in patients with diabetes mellitus and peripheral vascular disease: focus on skin and soft-tissue infections. *Clin Microbiol Infec* 2015;**21**(Suppl 2): S27−32.
38. Taupin P, Gandhi A, Saini S. Integra® dermal regeneration template: from design to clinical use. *Cureus* 2023;**15**:e38608.
39. Fagundes CT, Amaral FA, Teixeira AL, Souza DG, Teixeira MM. Adapting to environmental stresses: the role of the microbiota in controlling innate immunity and behavioral responses. *Immunol Rev* 2012;**245**:250−64.
40. Spragge F, Bakkeren E, Jahn MT, Araujo EBN, Pearson CF, Wang XD, et al. Microbiome diversity protects against pathogens by nutrient blocking. *Science* 2023;**382**:eadj3502.
41. Gardiner M, Vicaretti M, Sparks J, Bansal S, Bush S, Liu M, et al. A longitudinal study of the diabetic skin and wound microbiome. *Peerj* 2017;**5**:e3543.
42. Greenwood JE, Schmitt BJ, Wagstaff MJD. Experience with a synthetic bilayer biodegradable temporising matrix in significant burn injury. *Burns Open* 2018;**2**:17−34.
43. Guggenheim M, Zbinden R, Handschin AE, Gohritz A, Altintas MA, Giovanoli P. Changes in bacterial isolates from burn wounds and their antibiograms: a 20-year study (1986−2005). *Burns* 2009;**35**: 553−60.
44. Eming SA, Wynn TA, Martin P. Inflammation and metabolism in tissue repair and regeneration. *Science* 2017;**356**:1026−30.
45. Di Domizio J, Belkhodja C, Chenuet P, Fries A, Murray T, Mondéjar PM, et al. The commensal skin microbiota triggers type I IFN−dependent innate repair responses in injured skin. *Nat Immunol* 2020;**21**:1034−45.
46. Zhang J, Muri J, Fitzgerald G, Gorski T, Gianni-Barrera R, Masschelein E, et al. Endothelial lactate controls muscle regeneration from ischemia by inducing M2-like macrophage polarization. *Cell Metab* 2020;**31**. 1136-53.e7.
47. Louiselle AE, Niemiec SM, Zgheib C, Liechty KW. Macrophage polarization and diabetic wound healing. *Transl Res* 2021;**236**: 109−16.
48. Mouritzen MV, Petkovic M, Qvist K, Poulsen SS, Alarico S, Leal EC, et al. Improved diabetic wound healing by LFcinB is associated with relevant changes in the skin immune response and microbiota. *Mol Ther-meth Clin D* 2021;**20**:726−39.